

Simulation of Multi step DC-DC converter using APS Control for Fuel Cell Power System

DINESH K, KARTHIKEYAN N, DINAKARAN K P, MANIKANDAN C T, SUDHARSANAM S

Department of Electrical and Electronics Engineering
Panimalar Institute of Technology, Sri Venkateswara College of Engineering
Chennai-600 125, 602 105
INDIA

mailforkdinesh@gmail.com, karthiee27@gmail.com, dinakarankp@gmail.com,
manikandanct@yahoo.com, sudharsanam@svce.ac.in

Abstract: - This paper analyzes a novel pulse width modulation (PWM) scheme for alternate phase shift (APS) isolated boost converter with voltage booster for fuel cell power system by combining APS control and traditional isolated PWM control. The APS control is used to reduce the voltage stress on switching devices in light load while the traditional interleaving control is used to keep best performance in heavy load. The mathematical analysis is also presented to deliver the feasible power ranges. Based on the analytical calculations, a full range control combining APS and traditional isolated control is proposed. Zero voltage switching is achieved for alternate phase switches. Finally, it is verified by simulated results.

Key-Words: -Boost converter, Fuel cell, Interleaved, Loss breakdown, Voltage multiplier.

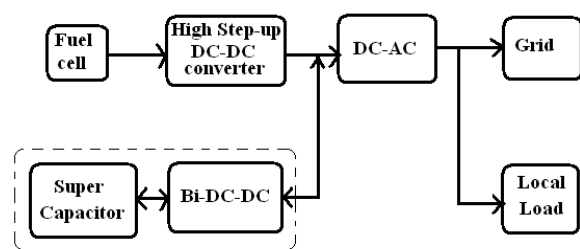
1 Introduction

With increasing concern about energy and environment, it is necessary to explore the non-conventional energy including wind, solar, fuel cell, etc. Fuel cell is one of the most needed choices due to its advantages of zero emission, low noise, high power density, and being easily modularized for portable power sources, hybrid electrical vehicles, distributed generation systems, etc. [1].

The grid-tied power system based on fuel cell is shown in Fig.1. For a typical 10-kW proton exchange membrane fuel cell, the output voltage is from 65 to 100V. However, the input voltage of the three phase dc/ac converter between fuel cell and the DC-DC converter between fuel cell and the DC-AS converter is need for the system as shown in Fig.1. The DC-DC converter will generate a peak frequency input current ripple, while will reduce the life time of the fuel cell stack [2]-[4]. In addition, the hydrogen energy decreases with increasing the current ripple of the fuel cell stack output [5]. Therefore, the switched mode power converter for the system as shown in Fig.1 should have high step-up ratios with minimum input current ripple.

High step-up ratio can be obtained by combining conventional boost converter with switched inductors [6], coupled inductors [7]-[9], high

frequency transformers [10], or switched capacitors [11]-[14], [19]. They can obtain high step-up ratio with high efficiency, low-voltage stress, and less electromagnetic interference. In order to reduce output fuel cell stack output current ripples or the DC-DC converter input current ripples, either a passive filter [15] or active filter [5] can be used, however, this will increase the difficulty of the system.



Power Management system

Fig.1 Grid-connected power system based on fuel cell

In fact, isolating the Switched mode Power Supply can minimizing the input current ripples of the DC-DC converter [16]. An isolated boost converter with voltage multipliers was proposed in [13]-[14]. Its voltage gain was increased up to $(M+1)$ times of the conventional boost converters with the same duty cycle D and lower voltage stresses. Wherefore, it has least input current ripples and output voltage

ripples in comparison to the conventional boost converter. The isolation of boost converter with voltage multipliers are shown in Fig.2.

The converter shown in Fig.2 can achieve least-voltage stress in the power devices, which increases the conversion efficiency. However, this is only true in heavy load when the voltage stresses of the power devices might increase when it works in discontinuous conduction mode (DCM) [17], which occurs when fuel cell only supplies a light load shown in Fig.2. In this case, higher voltage power devices need to be used, and therefore its cost and power loss will be increased.

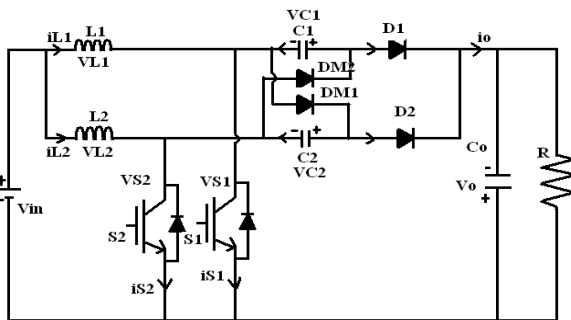


Fig.2 Structure of two-phase interleaved boost converter with voltage multiplier

These authors proposed a new pulse width modulation (PWM) control method, named as APS, to overcome the problem when the converter operates in light load [17], [18].

This paper investigates a modern PWM scheme for multi phase isolated boost converter with voltage multiplier for fuel cell power system by combining APS and conventional interleaving PWM control. The APS control is used to reduce the voltage stress on switches in light load while the traditional isolation control is used to keep better performance in heavy load. The boundary condition for exchanging between APS and traditional isolated PWM control is studied. Based on the aforementioned analysis, a wide power range control combining APS and traditional isolation control is proposed. Loss breakdown theory is also given to excel the efficiency of the converter. Finally, it is verified by simulation results.

2 Analysis with traditional interleaving control for low power operation

It is assumed that all components in the converter are ideal, both capacitor C_1 and C_2 are large enough,

and duty cycle is less than 0.5. The operation of a switching cycle of the converter can be divided into six stages at boundary condition which the voltage stress on switch will be large than half of the output voltage with traditional interleaving control, as shown in Fig.3. Typical theoretical waveforms at boundary condition are shown in Fig.4.

2.1 Stages of operation

When including a subsection you must use, for its heading, small letters, 12pt, left justified, bold, Times New Roman as here.

2.1.1 First stage (t_0, t_1)

At the moment of t_0 , both switch S_1 and S_2 are off, the energy stored in the inductor L_2 and capacitor C_2 in previous stage are transferred to the output capacitor C_0 through D_2 as shown in Fig. 3(a). The voltage stress on switch S_1 is the input voltage V_{in} , and the voltage stress on switch S_2 is $(V_o - V_{C2})$, where V_o is the output voltage and V_{C2} is the voltage of the capacitor C_2 .

2.1.2 Second stage (t_1, t_2)

At the moment of t_1 , the switch S_1 is turned ON, the inductor L_1 starts to store energy from zero as shown in Fig. 3(b). In the meantime, if $(V_{C1} + V_{C2}) < V_o$, where V_{C1} is the capacitor C_1 voltage, the diode D_2 will be turned OFF and the diode D_{M2} will be turned ON; therefore, the energy in the inductor L_2 will be transferred to the capacitor C_1 . If there is enough energy in the inductor L_2 , $V_{C1} + V_{C2} \geq V_o$. Then, the diode D_2 will be turned ON again, which is shown in Fig. If there is not enough energy to charge V_{C1} to $(V_o - V_{C2})$, then it will come to the Third stage as shown in Fig. 3(c). If there in the inductor L_2 is just discharged to zero and $V_{C1} + V_{C2} = V_o$ at the end of the stage, then we say that the circuit operates in the boundary condition state. During the stage, the voltage stress-on switch S_2 is V_{C1} .

2.1.3 Third stage (t_2, t_3)

At the moment of t_2 , the current in the inductor L_2 just falls to zero; all the diodes are in off state and the inductor L_1 is in charging state until the switch S_1 is turned OFF at the moment of t_3 . The voltage stress on switch S_2 is V_{in} . At the end of this stage, the current in the inductor L_1 comes to the peak value I_{L1P} ,

$$I_{L1P} = \frac{V_{in} D_m T_s}{L} \tag{1}$$

And where V_{in} is the input voltage, L is the inductance of L_1 and L_2 , D_m is the duty cycle at boundary condition, and T_s is the switching period.

2.1.4 Fourth stage (t_3, t_4)

At the moment of t_3 switch S_1 and S_2 are in off state, the energy in the inductor L_1 and the capacitor C_1 will be transferred to the output capacitor C_o through the diode D_1 , which is similar to first stage. In this stage, the voltage stress on switch S_1 is $(V_o - V_{C1})$, and the voltage stress on switch S_2 is V_{in} . At

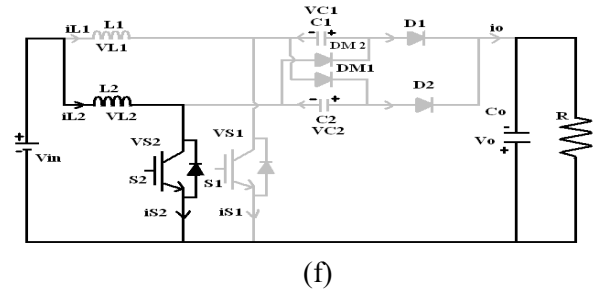
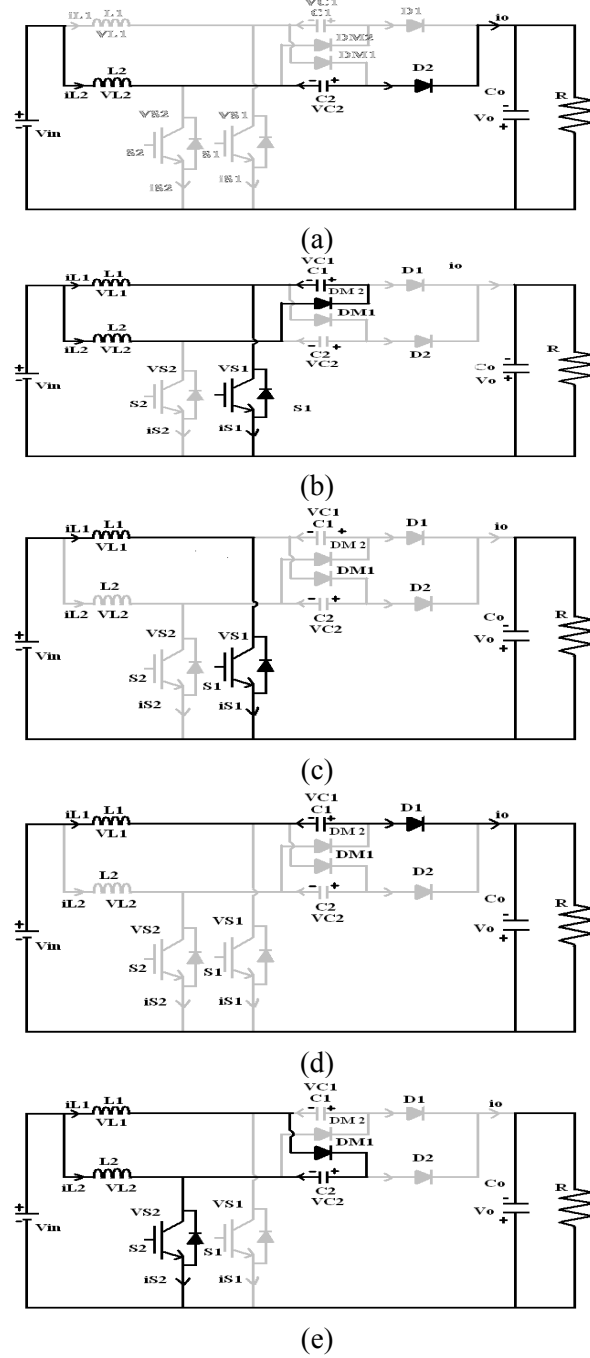


Fig. 3. Stages at boundary condition. (a) First stage (t_0, t_1), (b) second stage (t_1, t_2), (c) third stage (t_2, t_3), (d) fourth stage (t_3, t_4), (e) fifth stage (t_4, t_5), (f) sixth stage (t_5, t_6).

the end of this stage, the current in the inductor L_1 decreases to be I_{L1M} ,

$$I_{L1M} = I_{L1P} - \frac{V_o - V_{C1} - V_{in}(0.5 - D_m)T_s}{L} \quad (2)$$

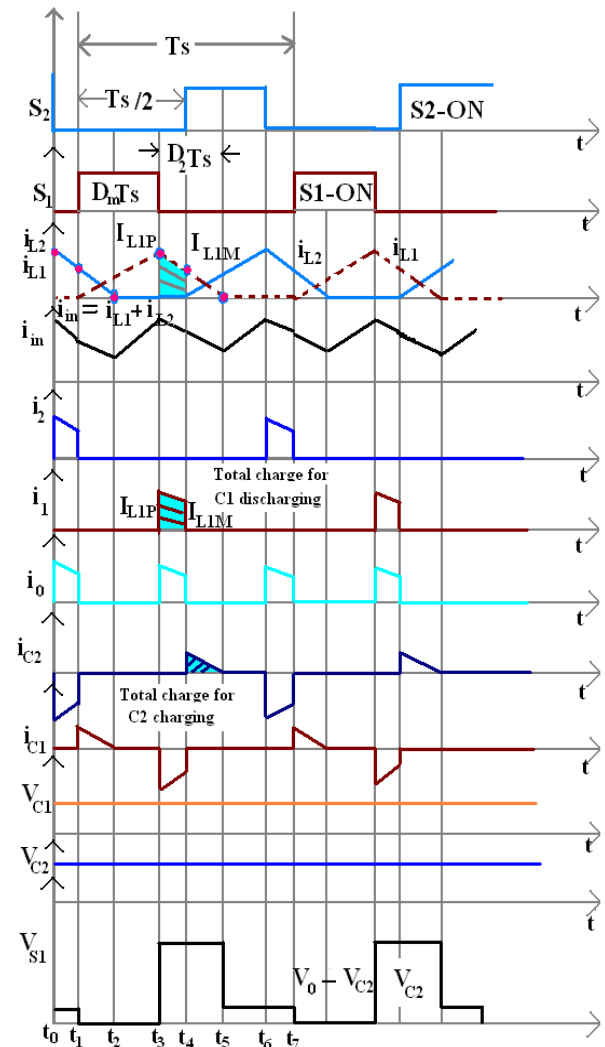


Fig. 4 Main theoretical waveforms at boundary condition.

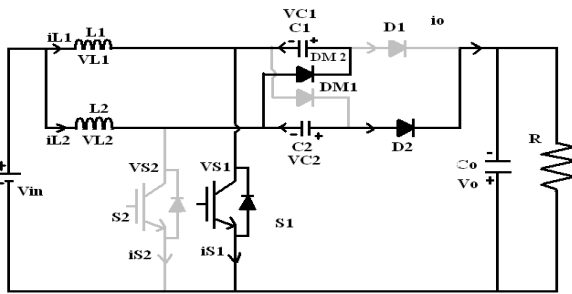


Fig.5 One Stage above boundary condition.

2.1.5 Fifth stage (t₄,t₅)

At the moment of t₄, the switch S₂ is turned ON and the inductor L₂ starts to store energy. This stage is similar to the second stage. In this stage, the voltage stress on switch S1 is V_{C2}. At the end of this stage, the current in the inductor L₁ decreases to zero from I_{L1M} and thus

$$I_{L1M} - \frac{V_{C2} - V_{in}}{L} (D_2 - 0.5 - D_m)T_s = 0 \quad (3)$$

Where D₂ is the duty cycle as shown in Fig.4

2.1.6 Sixth stage (t₅, t₆)

At the moment of t₅, the current in the inductor L₁ decreases to zero. All the diodes are in off state and the inductor L₂ is in charging state until the stage comes to the end at the moment t₆. A new switching period will begin with the next first stage.

From the aforementioned analysis, the voltage sum of capacitor C₁ and C₂ will be V_o at boundary condition. If it is less than V_o, the voltage stress on switch S1 and S2 will be larger than V_o/2, because the voltage stress on switch S1 is (V_o-V_{C1}) during the fourth stage and the voltage stress on switch S₂ is (V_o-V_{C2}) during the first stage.

The average value of the output current i_o is equal to the dc component of the load current V_o/R, then

$$\begin{aligned} \frac{V_o}{R} &= \frac{1}{T_s} \int_0^{T_s} (i_o) dt = \frac{1}{T_s} \int_0^{T_s} (i_1 + i_2) dt \\ &= \frac{1}{T_s} \int_0^{T_s} i_1 dt + \frac{1}{T_s} \int_0^{T_s} i_2 dt \end{aligned} \quad (4)$$

With the same parameter4s of the circuits in multi phases as shown in Fig.2, therefore

$$\frac{1}{T_s} \int_0^{T_s} i_1 dt = \frac{1}{T_s} \int_0^{T_s} i_2 dt \quad (5)$$

By merging equations (4) and (5), it is solved as,

$$\begin{aligned} \frac{V_o}{R} &= \frac{2}{T_s} \int_0^{T_s} i_1 dt = \frac{2}{T_s} \int_{t_3}^{t_4} i_1 dt \\ &= \frac{2}{T_s} \left[\frac{1}{2} (I_{L1P} + I_{L1M})(0.5 - D_m)T_s \right] \\ &= (I_{L1P} + I_{L1M})(0.5 - D_m) \end{aligned} \quad (6)$$

Where R is the load

At the boundary condition, the diode D₂ (D₁) approaches the conduction state during the second stage (fifth stage), which is shown in Fig.5.

The following equation can be obtained

$$V_{C1} + V_{C2} = V_o \quad (7)$$

Considering the capacitors C₁ and C₂ are quite enough, average voltage of the capacitor will keep equal. Otherwise, the converter will not operate at boundary condition, therefore

$$V_{C1} = V_{C2} = \frac{1}{2} V_o \quad (8)$$

By substituting (1) and (8) into (2), the current I_{L1M} can be obtained as,

$$I_{L1M} = \frac{V_{in} - \frac{V_o}{2} + V_o \cdot D_m}{2L} T_s \quad (9)$$

As shown in Fig.4, the total discharge of capacitor C1 between t₃ and t₄ is

$$Q_{C1} = \int_{t_3}^{t_4} i_{C1} dt = \frac{1}{2} (I_{L1P} + I_{L1M})(0.5 - D_m)T_s \quad (10)$$

The total charge of capacitor C₂ between t₄ and t₅ is

$$Q_{C2} = \int_{t_4}^{t_5} i_{C2} dt = \frac{1}{2} I_{L1M}(D_2 - 0.5 - D_m)T_s \quad (11)$$

According to the previous analysis, the total discharge of C1 is equal to the total charge of capacitor C2 at boundary condition. Therefore, there will be

$$Q_{C1} = Q_{C2} \quad (12)$$

By combining (10), (11), and (12), the following can be derived

$$D_2 = (0.5 - D_m) \left(\frac{I_{L1P}}{I_{L1M}} + 2 \right) \quad (13)$$

By combining (3) and (6) and then substituting (1), (9), and (13) into them, the boundary condition can be derived as,

$$\begin{cases} K = K_{crit} = \frac{n-2}{2n(n-\sqrt{2})^2} & (a) \\ D_{crit} = \frac{n-2}{2(n-\sqrt{2})} & (b) \end{cases} \quad (14)$$

Where n is the voltage gain of the converter ($n=V_o/V_{in}$), and K is the parameters of the circuit and $K=2L/(R \times T_s)$.

The boundary constraint with traditional interleaving control decided by (14) is shown in Fig.6. The constraint includes two parts: duty cycle D and the circuit parameters $K = 2L/(R \times T_s)$. As the switching period T_s and the input inductor L are designed at nominal operation in continuous conduction mode (CCM), the constraint is determined by duty cycle D and the load R . The reason why there are two parts in the boundary constraint is that the duty cycle D varies with the load when the converter operates in DCM. For a given application, the voltage gain of the dc/dc converter is determined. And then, the minimum duty cycle that can maintain low-voltage stress in main power devices with traditional interleaving control will be given by (14)-(b) and as shown in Fig. 6(a). At the same minimum duty cycle, the converter operates at boundary condition when the circuit parameters $K = 2L/(R \times T_s)$ satisfy (14)-(a) and as shown in Fig. 6(b).

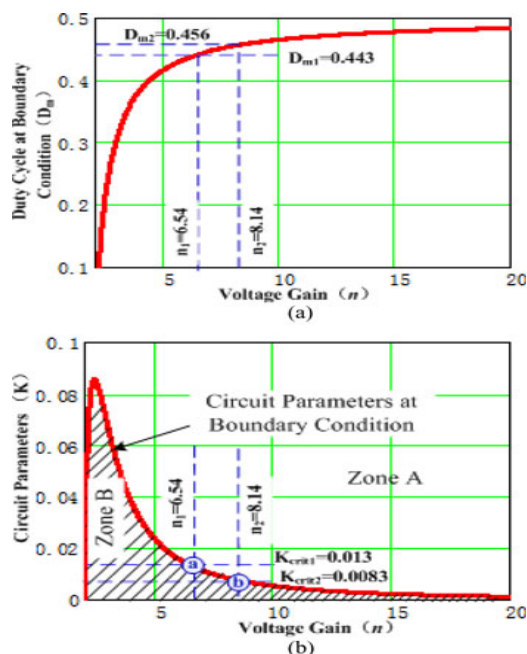


Fig. 6. Boundary constraint varies with voltage gain. (a) Duty cycle at boundary condition varies with voltage gain, (b) circuit parameters at boundary condition varies with voltage gain.

When the converter operates above the boundary condition, the circuit parameters are in Zone A of Fig. 6(b), i.e., $K > K_{crit}$, the converter could achieve halved voltage stress on switches with traditional interleaving control with the duty cycle above the solid red line as shown in Fig. 6(a). When

decreasing the load to the solid red line at boundary condition in Fig. 6(b), i.e., $K = K_{crit}$, the duty cycle of the converter will be decreased to the solid red line in Fig. 6(a). When decreasing the load further in Zone B in Fig. 6(b), i.e., $K < K_{crit}$, the duty cycle will be decreased further to be smaller than the minimum duty cycle that maintains low-voltage stress on switches with traditional interleaving control. Then, the APS control should be used to achieve halved voltage stress on switches in Zone B [17], [18].

In our 1-kW simulation design, the input voltage of the converter is 86–107 V, and the output voltage of the converter is 700 V. The voltage gain will vary from $n_1 = 6.54$ to $n_2 = 8.14$, and then the circuit parameters at boundary conditions K_{crit} will vary from $K_{crit1} = 0.013$ to $K_{crit2} = 0.0083$ as shown in Fig. 6(b), the duty cycle will vary from $D_{m1} = 0.443$ to $D_{m2} = 0.456$ in order to maintain the stable output voltage. When the circuit parameters $K = 2L/(R \times T_s)$ are below the solid red line from point a to point b at different voltage gain as shown in Fig. 6(b), the duty cycle will be decreased further to be less than the solid red line from $D_{m1} = 0.443$ to $D_{m2} = 0.456$ as shown in Fig. 6(a), and then the voltage stress on switches will be increased at this load. In order to achieve the halved voltage stress on switches at this load, APS control is needed.

3 Simulated Circuit

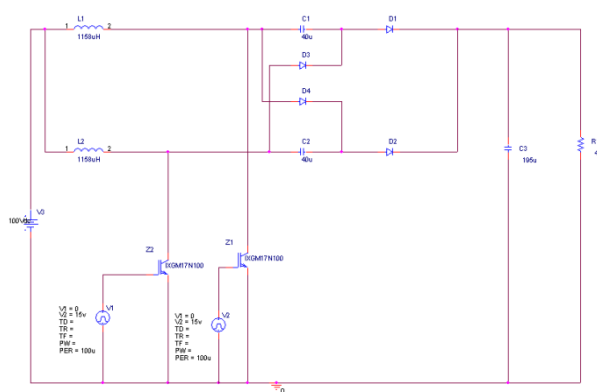


Fig. 7 Simulated circuit for multistep DC-DC converter

The multistep DC-DC converter is simulated with PSPICE 9.2 platform. The circuit has two main switches $S1$ and $S2$, two main diodes and two auxiliary diodes, input inductors, one output capacitor and two auxiliary capacitors and provided the resistive load of 478Ω. The circuit is operated for 1kW power capacity. The alternating

phase shift provides high power handling capability and improves the efficiency of switching devices.

4 Simulation Results

The input voltage of 100 V is applied to the multistep DC-DC converter and 600 V of output voltage is obtained in the simulated circuit it is shown in the Fig. 8

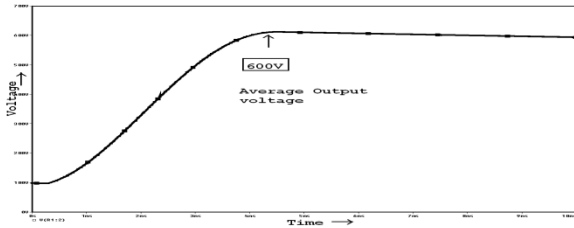


Fig. 8 Output voltage for the multistep DC-DC converter

The average output power is 800 Watts is obtained in the simulated circuit and it is utilized for fuel cell applications is shown in Fig.9

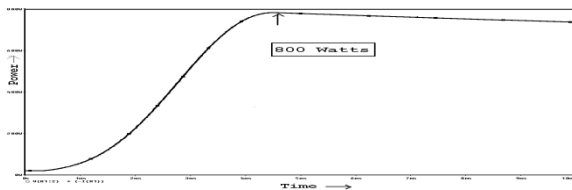
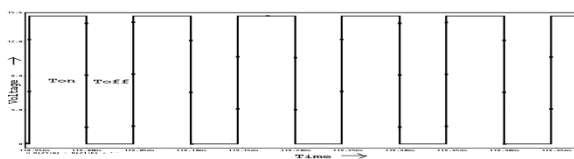
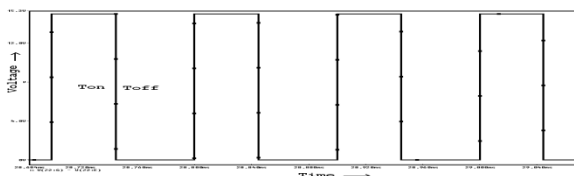


Fig. 9 Output power for the multistep DC-DC converter



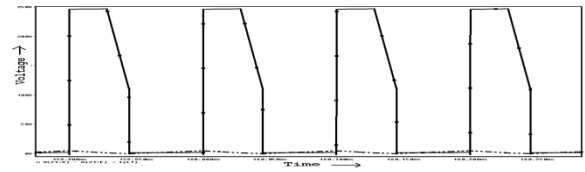
(a)



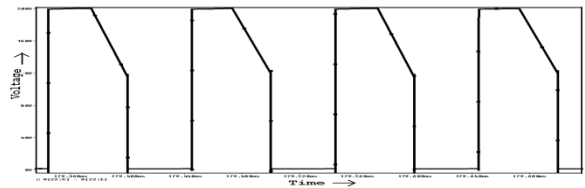
(b)

Fig. 10 Gate to emitter voltage for multistep DC-DC converter

A 15V gate pulse is applied to the main and auxiliary switches and is simulated for 200ms is shown in fig 10 (a) and (b).



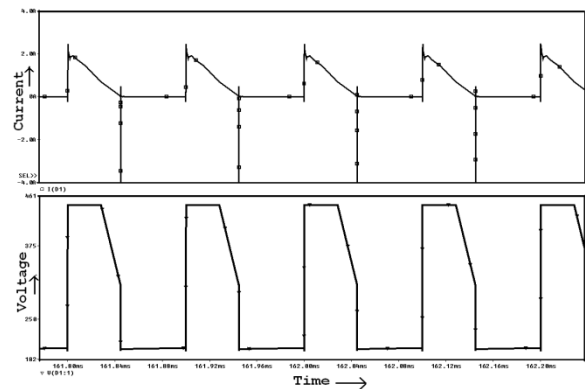
(a)



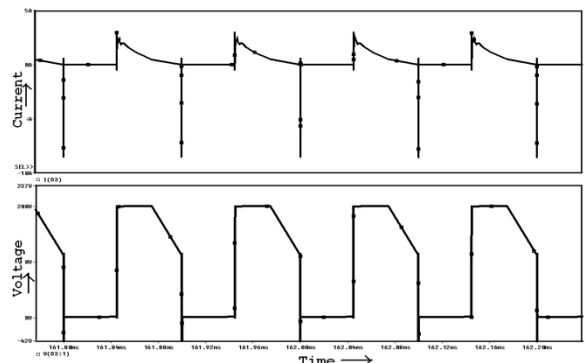
(b)

Fig. 11 Collector to emitter voltage for multistep DC-DC converter

The collector to emitter voltage of 240V is obtained in the multistep converter is shown in Fig 11 (a) and (b) the switching stress in conventional converter is much reduced by using the APS methodology.



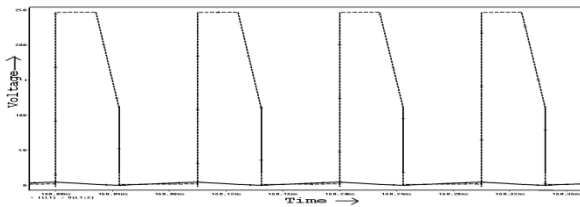
(a)



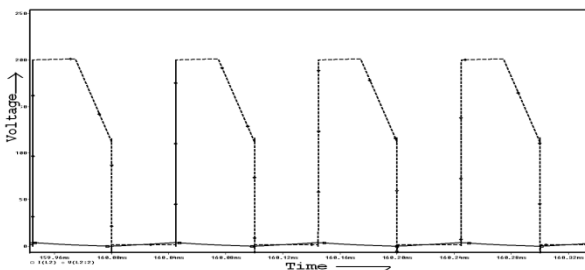
(b)

Fig 12. Main and auxiliary diode voltage and current waveforms

The diode voltage and current waveforms is shown in the Fig 12 (a) and (b) the voltage of 200V is obtained in the simulation results.



(a)



(b)

Fig.13 Inductor voltage and current waveforms

The inductor voltage of 230 V is obtained in the simulated circuit and it is shown in Fig 13

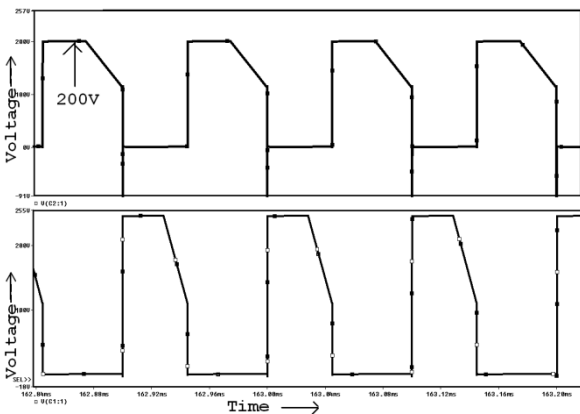
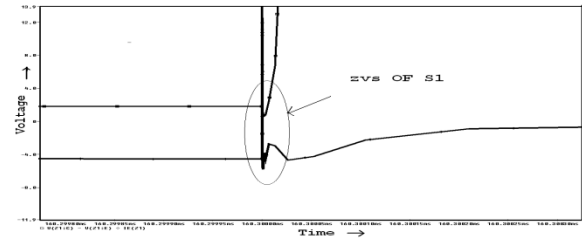
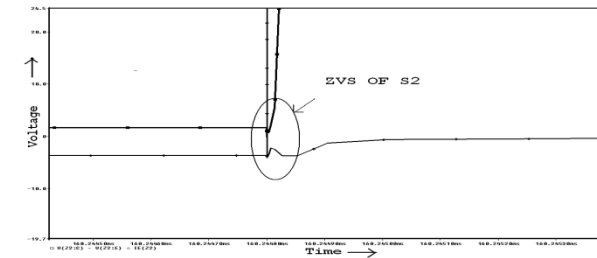


Fig. 14 Capacitor voltage waveforms

The auxiliary capacitor voltage of 200V is obtained in the simulated circuit and shown in the Fig.14



(a)



(b)

Fig. 15 Zero voltage switching of S₁ and S₂

The zero voltage switching is achieved for main and auxiliary switches. The switching efficiency of the converter is improved and thereby losses are reduced as shown in Fig.15

5 Conclusion

A simulation of Multistep DC-Dc converter for fuel cell power system has been proposed for a given voltage and power level. The existing converter has been modified by series and parallel legs of switches. The modes of operation, analysis, design and simulation results have been presented for a 600V, 1 HP load. For both the converters, it is observed that ZVS turn-on and turn-off of the active switches. In addition to that voltage stresses in the switches have been reduced and efficiency of the converter is also improved compared to hard switching topologies.

References:

- [1] N. Sammes, *Fuel Cell Technology: Reaching towards commercialization*, U.K.: Springer-Verlag, 2006.
- [2] G. Fontes, C. Turpin, S. Astier and T. A. Meynard, Interactions between fuel cells and power converters: Influence of current harmonics on a fuel cell stack, *IEEE Trans. Power Electron.*, vol.22, no.2, pp.670-678, Mar.2007.
- [3] P. Thounthong, B. Davat, S. Rael, and P. Sethakul, Fuel starvation, *IEEE Ind.*

- Appl. Mag.*, vol. 15, no.4, pp.52-59, Jul./Aug. 2009.
- [4] S. Wang, Y. Kenarangui, and B. Fahimi, Impact of boost converter switching frequency on optimal operation of fuel cell systems, in *Proc. IEEE vehicle power propulsion cong.*, 2006, pp. 1-5.
- [5] S.K. Mazumder, R.L. Burra, and K. Acharya, A ripple-mitigating and energy-efficient fuel cell power-conditioning system, *IEEE Trans. Power Electron.*, vol. 22, no.4, pp. 1437-1452, Jul. 2007.
- [6] B. Axelrod, Y. Berkovich, and A. Ioinovici, Switched capacitor/switched-inductor structures for getting transformerless hybrid DC-DC PWM converters, *IEEE Trans. Circuits Syst, I: Reg. Papers*, vol. 55, no.2, pp.687-696, Mar. 2008.
- [7] Z./ Qun and F. C. Lee, High efficiency, high step-up DC-DC converters, *IEEE Trans. Power Electron.*, vol. 18, no. 1, pp.65-73, Jan. 2003.
- [8] H. Yi-Ping, C. Jiann-Fuh, L. Tsorng-Juu, and Y. Lung-Sheng, A novel high step-up converter for a micro grid system, *IEEE Trans. Power Electron.*, vol.26, no.4, pp. 1127-1136, Apr. 2011.
- [9] L. Wuhua, F. Lingli, Z. Yi, H. Xiangning, X. Dewei, and W. Bin, High step-up and high-efficiency fuel-cell power generation system with active clamp flyback-forward converter, *IEEE Trans. Ind. Electron.*, vol. 59, no.1, pp. 599-610, Jan.2012.
- [10] Y. Changwoo, K. Joongeun, and C. Sewan, Multiphase DC-DC converters using a boost-half bridge cell for high-voltage and high-power applications, *IEEE Trans. Power Electron.*, vol. 26, no. 2, pp. 381-388, Feb. 2011.
- [11] R. D Middlebrook, Transformerless DC-to-DC converters with large conversion ratios, *IEEE Trans. Power Electron.*, vol. 3, no.4, pp. 484-488, Oct. 1988.
- [12] A. A. Fardoun and E. H. ismail, Ultra step-up DC-DC converter with reduced switch stress, *IEEE Trans. Ind. Appl.*, vol. 46, no.5, pp. 2025-2034, Sep./Oct. 2010.
- [13] M. Prudente, L. L. Pfitscher, G. Emmendoerfer, E. F. Romaneli, and R. Gules, Voltage multiplier cells applied to non-isolated DC-DC converters, *IEEE Trans. Power Electron.*, vol.23, no.2, pp/ 871-887, Mar. 2008.
- [14] R. Gules, L. L. Pitscher, and L. C. Franco, An interleaved boost DC-DC converter with large conversion ratio, in *Proc. IEEE Int. Symp. Ind. Electron.*, 2003, pp. 411-416.
- [15] A. Shahin, M. Hinaje, J. Martin, S. Pierfederici, X. Rae, S. L. Rael, and B. Davat, High voltage ration DC-DC converter for fuel cell applications, *IEEE Trans. Ind. Electron.*, vol. 57, no.12, pp/ 3944-3955, Dec. 2010.
- [16] P. Thounthong, P. Sethakul, X. Rae, S.L. Rael, and B. Davar, Fuel cell current ripple mitigation by interleaved technique for high power applications, in *Proc. IEEE Ind. Appl. Soc. Annu. Meeting. Houston, TX, USA, 2009*, pp. 1-8.
- [17] X. Wu, L. Zhang, G. Shen, M. Shen, D. Xu and A. Ioinovici, A novel control method for light-loaded multiphase boost converter with voltage multiplier used as a front-end of a grid-connected fuel-cell generation, in *Proc. IEEE Energy convers. Congr. Expo., Phoenix, AZ, USA, 2011*, pp. 413-420.
- [18] L. Zhang, G. Shen, M. Chen, A. Ioinovici, and Dehong Xu, Two-phase interleaved boost converter with voltage multiplier under APS control method for fuel cell power system, in *Proc. 7th Int. Power Electron. Motion control Conf.*, Jun. 2-5. 2012, vol.2, pp. 963-967.
- [19] S. Lee, P. Kim and Sewan Choi, High step-up soft-switched converters using voltage multiplier cells, *IEEE Trans. Power Electron.*, vol. 28, no. 7, pp/ 3379-3387, Jul. 2013.